Random Lasers with Coherent Feedback

Hui Cao

Department of Physics and Astronomy, Materials Research Center
Northwestern University, Evanston, IL 60208-3112, USA
h-cao@northwestern.edu

Abstract. We have demonstrated lasing with resonant feedback in active random media. Recurrent light scattering provides coherent feedback for lasing. A detailed experimental study of laser emission spectra, spatial distribution of laser intensity, dynamics, and photon statistics of random lasers with coherent feedback is presented. The fundamental difference and transition between a random laser with resonant feedback and a random laser with nonresonant feedback are illustrated. We have achieved spatial confinement of laser light in micrometer-sized random media. The optical confinement is attributed to disorder-induced scattering and interference. Using the finite-difference time-domain method, we simulate lasing with coherent feedback in active random media.

1 Introduction

Optical scattering in a random medium may induce a phase transition in the photon transport behavior [1]. When the scattering is weak, the propagation of light can be described by a normal diffusion process. With an increase in the amount of scattering, recurrent light scattering events arise. Interference between the counterpropagating waves in a disordered structure gives rise to the enhanced backscattering, also called weak localization [2,3]. When the amount of scattering is increased beyond a critical value, the system makes a transition into a localized state. Light propagation is inhibited due to interference in multiple scattering [4,5,6,7,8,9]. This phenomenon is called Anderson localization of light. It is an optical analog to Anderson localization of electrons in solids [10].

Apart from the remarkable similarities, there are striking differences between electron transport and photon transport in a disordered medium. For example, the number of electrons is always conserved, whereas the number of photons may not be. In an amplifying random medium, a photon may induce the stimulated emission of a second photon. A fascinating phenomenon, which would never occur in an electronic system, is the lasing action in a disordered gain medium. Such lasers are called random laser. There are two kinds of random lasers: one has nonresonant (incoherent) feedback, the other has resonant (coherent) feedback. I will first introduce the two kinds of random lasers and explain the difference between them. Then, I will focus on our study of random lasers with resonant feedback.

V. M. Shalaev (Ed.): Optical Properties of Nanostructured Random Media,
Topics Appl. Phys. **82**, 303–330 (2002)

2 Two Kinds of Random Lasers

Lasing with nonresonant feedback occurs in the diffusive regime [11,12,13,14]. In a disordered medium, light is scattered and undergoes a random walk before leaving the medium. In the presence of gain, a photon may induce the stimulated emission of a second photon. When the gain length is equal to the average length of light path in the medium, the probability that a photon generates second photon before leaving the gain medium approaches one. Thus the photon density increases. From the theoretical point of view, the solution to the diffusion equation, including optical gain, diverges [15]. This phenomenon is similar to neutron scattering in combinations of nuclear fission.

When optical scattering is strong, light may return to a scatterer from which it is scattered before, and thereby form a closed loop path. When the amplification along such a loop path exceeds the loss, laser oscillation could occur in the loop which serves as a laser resonator. The requirement that the phase shift along the loop is equal to a multiple of 2π determines the oscillation frequencies. This is a random laser with coherent feedback [16,17,18]. Of course, the picture of a closed loop is intuitive but naive. The light may come back to its original position through many different paths. All of the backscattered light waves interfere and determine the lasing frequencies. Thus, a random laser with coherent feedback is a randomly distributed feedback laser. The feedback is provided by disorder-induced scattering.

Experimentally, we have observed the difference in the two kinds of random lasers and the transition between them [19]. The random medium we used in our experiment is a laser dye solution containing nanoparticles. The advantage of the suspension is that the gain medium and the scattering elements are separated. Thus, we can independently vary the amount of scattering by particle density and the optical gain by dye concentration.

Experimentally, rhodamine 640 perchlorate dye and zinc oxide (ZnO) particles are mixed in methanol. The ZnO particles have a mean diameter of 100 nm. To keep the particles from clustering, the solution, contained in a flask, is shaken in an ultrasonic cleaner for 20 minutes right before the photoluminescence experiment. The frequency-doubled output ($\lambda = 532$ nm) of a mode-locked Nd:YAG laser (10 Hz repetition rate, 25-ps pulse width) is used as pump light. The pump beam is focused by a lens (10 cm focal length) onto the solution contained in a 1 cm $\times$ 1 cm $\times$ 3 cm cuvette at nearly normal incidence. Emission in the direction $\sim 45^\circ$ from the normal of the cell front window is collected by a fiber bundle and directed to a 0.5-m spectrometer with a cooled CCD detector array.

By changing the ZnO particle density in the solution, we continuously vary the amount of scattering. Figure 1 shows the evolution of the emission spectra with the pump intensity when the ZnO particle density is $\sim 2.5 \times 10^{11}$ cm^{-3}. The dye concentration is fixed at 5×10^{-3} M. When the pump intensity exceeds a threshold, drastic spectral narrowing occurs. As shown in the insets

of Fig. 1, when the incident pump pulse energy exceeds ~ 3 μJ, the emission line width is quickly reduced to ~ 5 nm; meanwhile, the peak intensity increases much more rapidly with the pump power because optical scattering by the ZnO particles increases the path length of the emitted light inside the gain region. As the pump power increases, the gain length is reduced. Eventually the gain length at frequencies near the maximum of the gain spectrum approaches the average path length of photons in the gain regime. Then, a photon generates a second photon by stimulated emission before leaving the gain medium; thus the photon density increases dramatically. The sudden increase of emission intensity at frequencies near the maximum of the gain spectrum results in drastic narrowing of the emission spectrum. This process is lasing with nonresonant feedback.

Next, we keep the same dye concentration and increase the ZnO particle density to $1 \times 10^{12}\,\mathrm{cm}^{-3}$. Figure 2 plots the evolution of the emission spectra with pump intensity. We can see that the phenomenon becomes very different in strong scattering. When the incident pump pulse energy exceeds 1.0 μJ, discrete peaks emerge in the emission spectrum. The line width of these peaks is less than 0.2 nm, which is more than 50 times smaller than the line width of the amplified spontaneous emission (ASE) below the threshold. When the pump intensity increases further, more sharp peaks appear. As shown in the inset of Fig. 2, when the pump intensity exceeds the threshold where discrete peaks emerge in the emission spectrum, the emission intensity increases much more rapidly with the pump power. Hence, lasing occurs in the random cavities formed by recurrent light scattering. The phase relationship of the backscattered light determines the lasing frequencies. Laser emission from the random cavities results in discrete narrow peaks in the emission spectrum. Because the ZnO particles are mobile in the solution, the frequencies of the lasing modes change from pulse to pulse. The emission spectra in Figs. 1 and 2 are taken for a single pump pulse. When the pump power increases further, the gain exceeds the loss in more random cavities. Laser oscillation in these cavities gives additional peaks in the emission spectrum.

Next, we study the transition from lasing with nonresonant feedback to lasing with resonant feedback. Figure 3 shows the evolution of the emission spectra with the pump intensity when the ZnO particle density is $\sim 5 \times 10^{11}\,\mathrm{cm}^{-3}$. As the pump power increases, a drastic spectral narrowing occurs first. Then at higher pump intensity, discrete narrow peaks emerge in the emission spectrum. Because the amount of scattering in the solution is between the previous two cases, there is some but not a large probability that a photon is scattered back to the same scatterer from which it is scattered before. In other words, the random cavities formed by recurrent scattering are quite lossy. The pump intensity required to reach the lasing threshold in these cavities is high. Thus, the pump intensity first reaches the threshold where the gain length near the maximum of the gain spectrum becomes equal to the average path length of photons in the excitation volume. A significant

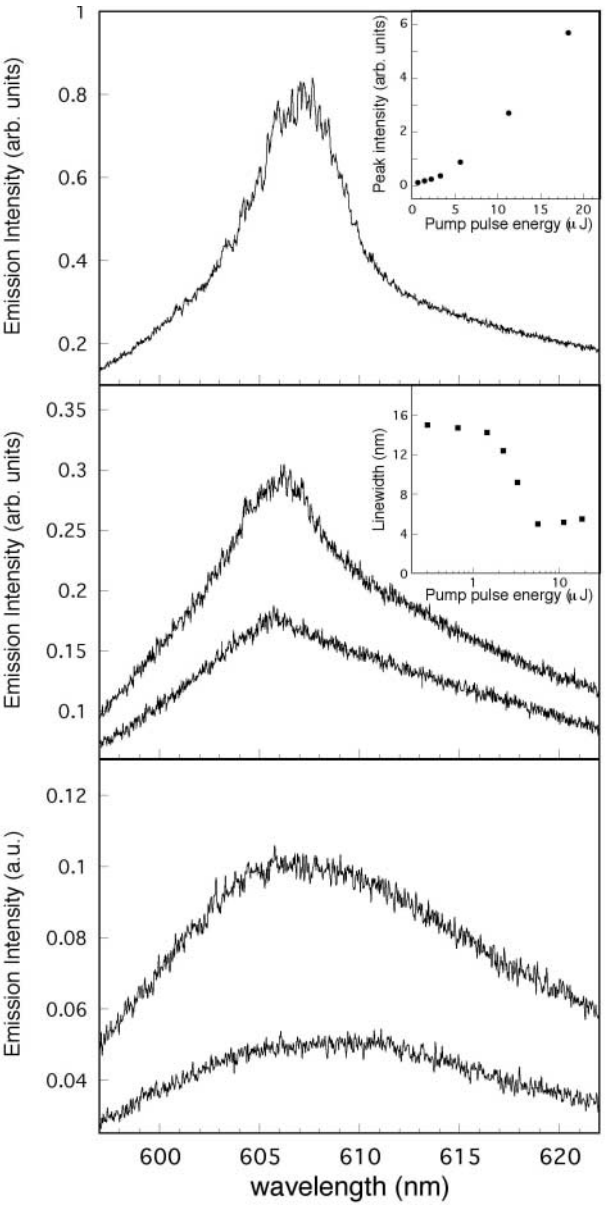

Fig. 1. Emission spectra when the incident pump pulse energy is (from bottom to top) 0.68, 1.5, 2.3, 3.3, 5.6 μJ. The ZnO particle density is $\sim 2.5 \times 10^{11}\,\mathrm{cm}^{-3}$. The *upper inset* is the emission intensity at the peak wavelength versus the pump pulse energy. The *lower inset* is the emission line width versus the pump pulse energy

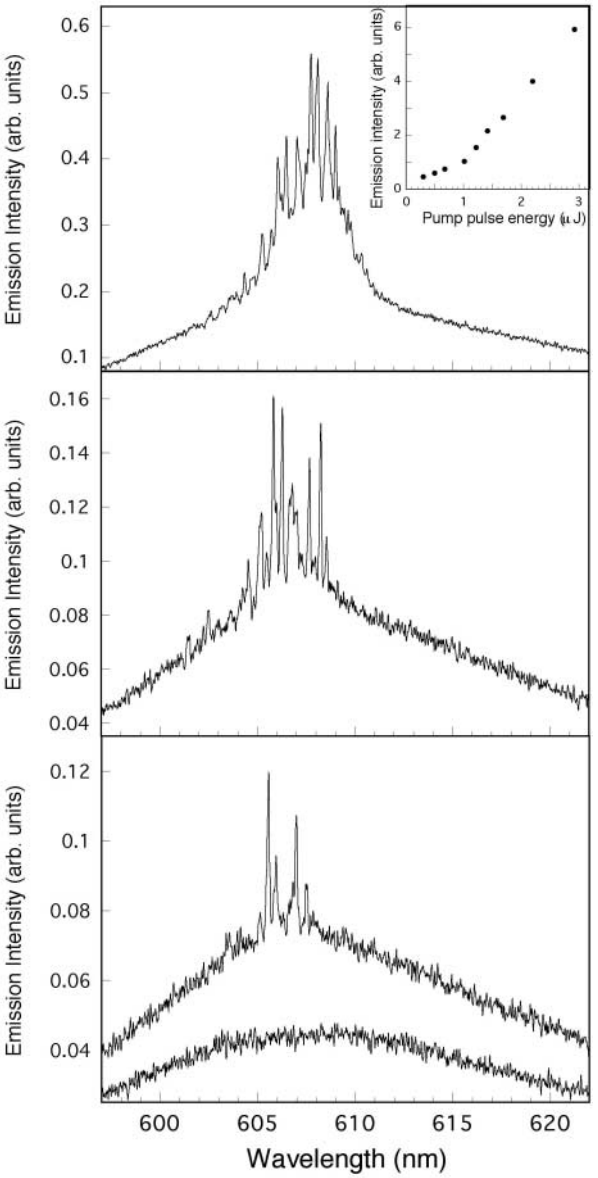

Fig. 2. Emission spectra when the incident pump pulse energy is (from bottom to top) 0.68, 1.1, 1.3, 2.9 μJ. The ZnO particle density is $\sim 1 \times 10^{12}\,\mathrm{cm}^{-3}$. The *inset* shows the emission intensity versus the pump pulse energy

spectral narrowing and a sudden increase of peak emission intensity occur, similar to what happens in Fig. 1. Then, the pump intensity reaches a second threshold where the gain exceeds the loss in some random cavities. Lasing oscillation occurs in these cavities, adding discrete peaks to the emission spectrum. However, the number of lasing modes in Fig. 3 is less than that in Fig. 2 under similar pump power. When the gain length and excitation volume are the same, a fewer number of scatterers leads to weaker optical scattering. Hence, the number of random cavities where the lasing threshold can be reached is smaller.

Therefore, there are two kinds of lasing processes in an active random medium, and they correspond to two lasing thresholds [19]. From the ray optics point of view, lasing with nonresonant feedback corresponds to the instability of light amplification along *open* trajectories in a random medium, and lasing with resonant feedback corresponds to the instability of light amplification along *closed* paths formed by recurrent scattering. An alternative and perhaps more accurate explanation for random lasers is based on quasi-states. Quasi-states are the eigenmodes of the Maxwell equations in a finite-sized random medium. When photons in a quasi-state reach the boundaries of the random medium, they are either reflected back to the medium or transmitted into the air. The transmitted photons are lost, and the reflected photons may enter other quasi-states. Hence, the decay of a quasi-state results from both light leakage through the boundaries and energy exchange with other quasi-states. When $kl > 1$ (k is a wave vector, l is the transport mean free path), the average decay rate of a quasi-state is larger than the average frequency spacing of adjacent quasi-states. Hence, the quasi-states are spectrally overlapped, giving a continuous emission spectrum.

In weak scattering, the quasi-states decay fast, and they are strongly coupled. Because of photon exchange among quasi-states, the loss of a set of interacting quasi-states is much lower than the loss of a single quasi-state. In an active random medium, when the optical gain for a set of interacting quasi-states at maximum gain reaches the loss of these coupled quasi-states, the total photon number in these coupled states builds up. The drastic increase of photon number at the frequency of maximum gain results in a significant spectral narrowing, as shown in Fig. 1.

With an increase in the amount of optical scattering, the dwell time of light in the random medium increases, and the mixing of the quasi-states is reduced. Hence, the decay rates of the quasi-states decrease. When the optical gain increases, it first reaches the threshold for lasing in a set of coupled quasi-states at maximum gain. As the optical gain increases further, it exceeds the loss of a quasi-state that has a long lifetime. Then, lasing occurs in a single quasi-state. The spectral line width of the quasi-state is reduced dramatically above the lasing threshold. A further increase of optical gain leads to lasing in more low-loss quasi-states. Laser emission from these quasi-states gives discrete peaks in the emission spectrum, as shown in Fig. 3.

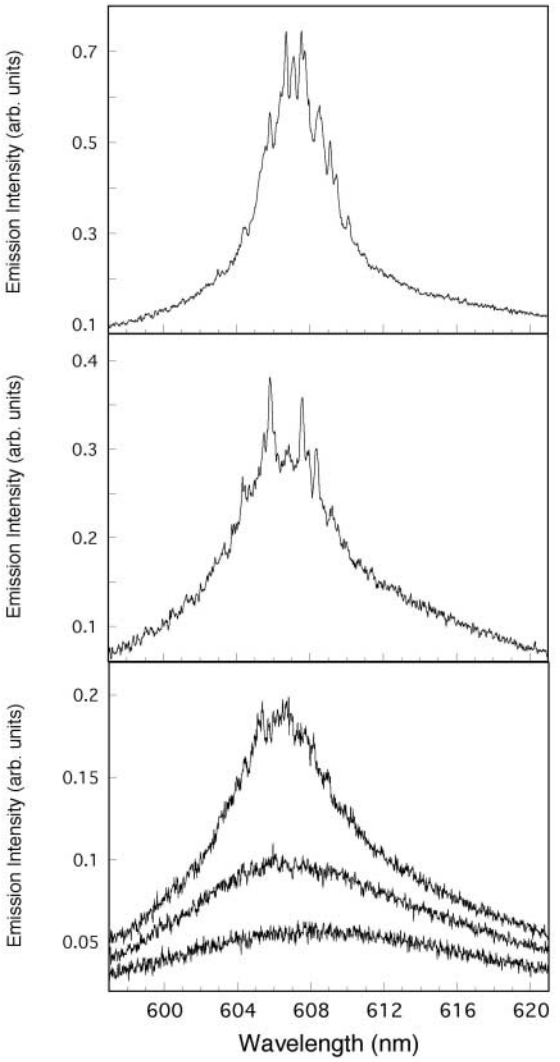

Fig. 3. Emission spectra when the incident pump pulse energy is (from bottom to top) 0.74, 1.35, 1.7, 2.25, and 3.4 μJ. The ZnO particle density is $\sim 6 \times 10^{11}\,\mathrm{cm}^{-3}$

When the scattering strength increases further, the decay rates of the quasi-states and the coupling among them continue decreasing. Because of the wide distribution of the decay rates of quasi-states, the threshold gain for lasing in individual low-loss quasi-states becomes lower than the threshold gain for lasing in the coupled quasi-states at maximum gain. Thus, lasing with resonant feedback occurs first, as shown in Fig. 2.

There has been much study of random lasers with nonresonant feedback [20,21]. Next, I will focus on our investigation of random lasers with resonant feedback.

3 Random Lasers with Resonant Feedback

In this section, I will present a quantitative study of random lasers with resonant feedback. To confirm that the coherent feedback is indeed provided by light scattering, we measured the dependence of the lasing threshold on the transport mean free path.

Because of the sedimentation of particles from the solution, the suspension was not suitable for quantitative measurement. Hence, we switched to a solid random medium and fabricated PMMA films containing rhodamine 640 perchlorate dye and TiO_2 particles. The average size of TiO_2 particles was 400 nm. By varying the TiO_2 particle density in the polymer film, we changed the scattering length. We fabricated a series of PMMA films with the same dye concentration but different particle density. The TiO_2 particle density in the polymer films varied from 8×10^{10} to $6 \times 10^{12}\,\mathrm{cm}^{-3}$. The lasing threshold in these films was measured under identical conditions. To characterize the transport mean free path in these films, we conducted coherent backscattering experiments [2,3]. The output from a He:Ne laser was used as the probe light since its wavelength is very close to the emission wavelength of rhodamine 640 perchlorate dye. To avoid absorption of the probe light, we fabricated PMMA films which contained only TiO_2 particles but not the dye. From the angular width of the backscattering cone, we estimated the transport mean free path l, after taking into account the internal reflection [22].

Figure 4 plots the incident pump pulse energy at the lasing threshold versus the transport mean free path. The dye concentration in the polymer film is fixed at $5 \times 10^{-2}\,\mathrm{M}$. With an increase of the TiO_2 particle density in the polymer film, the transport mean free path decreases, and the lasing threshold also decreases. The strong dependence of the lasing threshold on the transport mean free path clearly illustrates the important contribution of scattering to lasing. With an increase in the amount of optical scattering, the feedback provided by scattering becomes stronger. The quasi-states of the random medium have lower loss. Thus, the lasing threshold is reduced. Through curve fitting, we found that the incident pump intensity at the lasing threshold is proportional to the square root of the transport mean free path. Figure 5 shows the number of lasing modes in the samples with different scattering lengths at the same pump intensity. The stronger the scattering, the more lasing modes emerge, because in a random medium with stronger scattering strength, there are more low-loss quasi-states. Hence, when the optical gain is fixed, lasing occurs in more quasi-states. An interesting feature in Figs. 4 and 5 is that when the transport mean free path approaches the optical wavelength, the lasing threshold pump intensity drops quickly, and

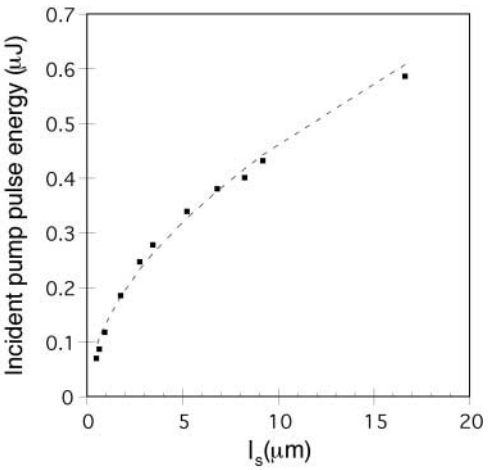

Fig. 4. The incident pump pulse energy at the lasing threshold versus the transport mean free path l_s in PMMA films. The *dashed line* is the fitted curve represented by $P_{th} = 0.13/l_s^{0.53}$

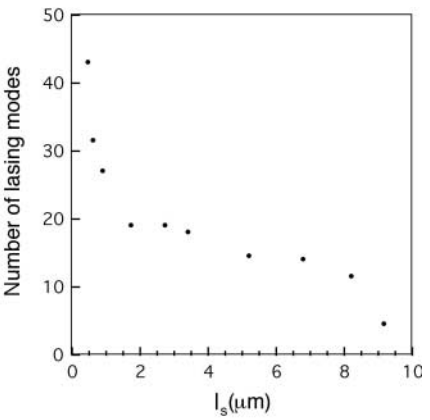

Fig. 5. The number of lasing modes as a function of the scattering length l_s in PMMA films. The incident pump pulse energy is 1.0 μJ

the number of lasing modes increases dramatically. Therefore, the regime of $l \sim \lambda$ is important to both fundamental physics and practical application. Next, I will discuss random lasers in the regime $l \leq \lambda$. To achieve such a short scattering mean free path, we used ZnO powder and polycrystalline thin films to increase the contrast of refractive indexes in the binary random medium.

ZnO films are deposited on sapphire or amorphous fused silica substrates by laser ablation. A pulsed KrF excimer laser (248 nm) is used to ablate a hot pressed ZnO target in an ultrahigh vacuum chamber. A detailed description of the growth apparatus and growth procedure can be found in [23]. We took

transmission electron microscopy (TEM) images of the ZnO films. From the plane view TEM image, the ZnO film consists of many irregularly-shaped grains whose sizes vary from 30 to 130 nm. The cross-sectional TEM image reveals that the grains have straight sidewalls that are perpendicular to the substrate. Hence, the polycrystalline film is a 2-D random medium. The in-plane randomly oriented polycrystalline grain structure results in strong optical scattering in the plane of the film [16,24]. The optical confinement in the direction perpendicular to the film is achieved through index guiding, similar to 2-D photonic crystals.

ZnO powder is a 3-D random medium [17,25]. The ZnO nanoparticles are synthesized by a precipitation reaction. The process involves hydrolysis of a zinc salt in a polyol medium. Through the process of electrophoresis, ZnO powder films are made on ITO-coated substrates. The film thickness varies from a few to 50 μm. Figure 6a is a scanning electron microscope (SEM) image of the ZnO particles. The average particle size is about 50 nm.

We characterized the transport mean free path l in the coherent backscattering experiment [2,3]. ZnO has a direct band gap of 3.3 eV. To avoid absorption, the frequency-doubled output ($\lambda = 410$ nm) of a mode-locked Ti:Sapphire laser (76 MHz repetition rate, 200 fs pulse width) was used as

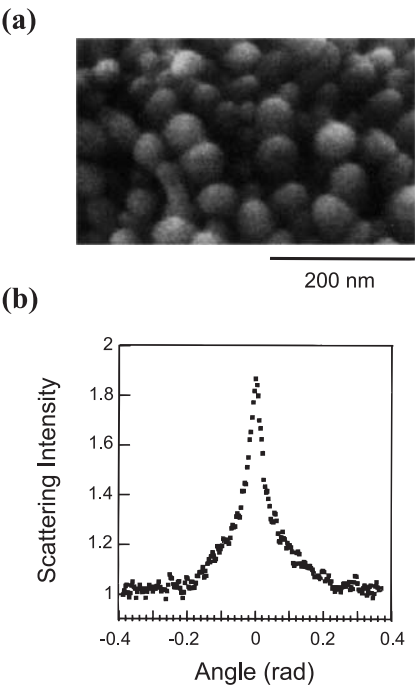

Fig. 6. (**a**) SEM image of the ZnO nanoparticles. (**b**) Measured backscattering cone from the ZnO powder film

the probe light. Figure 6b shows the measured backscattering cone of the ZnO powder film. From the angle of cusp, we estimated that $l \approx 0.5\lambda$, after taking internal reflection into account [22].

In the photoluminescence experiment, the ZnO powder film is optically pumped by the fourth harmonic ($\lambda = 266\,\text{nm}$) of a mode-locked Nd:YAG laser. The pump beam is focused to a $\sim$ 20-μm spot on the film surface with normal incidence. Electrons in the valence band absorb pump photons and jump to the conduction band. They subsequently relax to the bottom of the conduction band before radiative decay. The spectrum of emission from the powder film is measured by a spectrometer with 0.13-nm spectral resolution. At the same time, the spatial distribution of the emitted light intensity in the film is imaged by an ultraviolet (UV) microscope onto a UV-sensitive charge-coupled device (CCD) camera. The amplification of the microscope is about 100 times. The spatial resolution is around 0.24 μm. A band-pass filter is placed in front of the microscope objective to block the pump light.

Figure 7 shows the measured emission spectra and spatial distribution of emission intensity in a ZnO powder film at different pump intensities. At low pump intensity, the spectrum consists of a single broad spontaneous emission peak. Its full width at half maximum (FWHM) is about 12 nm (Fig. 7a). As shown in Fig. 7b, the spatial distribution of the spontaneous emission intensity is smooth across the excitation area. Due to the variation in pump intensity over the excitation spot, the spontaneous emission in the center of the excitation spot is stronger. When the pump intensity exceeds a threshold, very narrow discrete peaks emerge in the emission spectrum (Fig. 7c). The FWHM of these peaks is about 0.2 nm. Simultaneously, bright tiny spots appear in the image of the emitted light distribution in the film (Fig. 7d). The sizes of the bright spots were between 0.3 and 0.7 μm. When the pump intensity is increased further, additional sharp peaks emerge in the emission spectrum. Correspondingly, more bright spots appear in the image of the emitted light distribution. The frequencies of the sharp peaks depend on the sample position. When we move the pump beam spot across the sample, the frequencies of the sharp peaks change. Figure 8 plots the spectrally integrated emission intensity as a function of pump intensity. A threshold behavior is clearly seen: above the pump intensity at which multiple sharp peaks emerge in the emission spectrum, the integrated emission intensity increases much more rapidly with pump intensity.

We also measured the temporal profile of the emission from the ZnO powder film with a Hamamatsu streak camera. The temporal resolution of the streak camera is 2 ps. The scattered pump light is blocked by the input optics of the streak camera.

Figure 9 shows the temporal evolution of emission below the lasing threshold, just above the lasing threshold, and well above the lasing threshold. Below the lasing threshold, the spontaneous emission decay time is 167 ps. When the pump intensity exceeds the lasing threshold, the emission pulse is

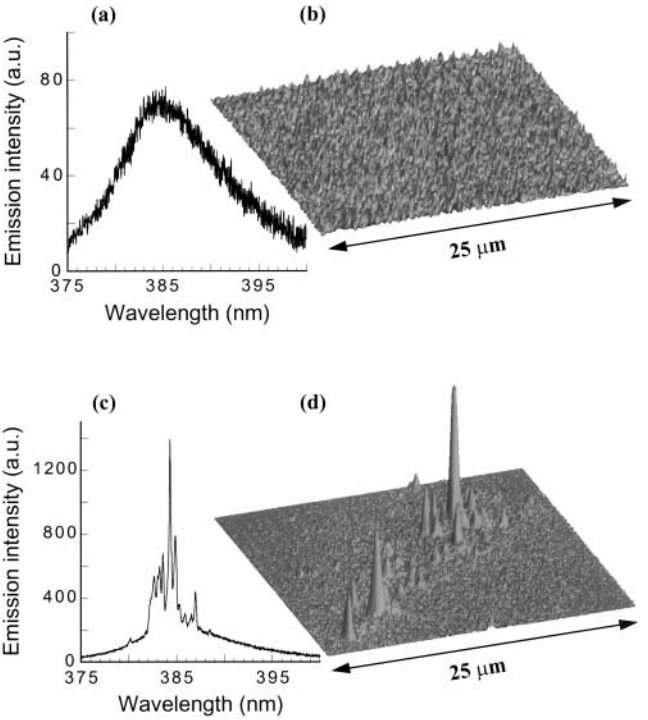

Fig. 7. (**a**) and (**c**) The measured spectra of emission from the ZnO powder film. (**b**) and (**d**) The measured spatial distribution of emission intensity in the film. The incident pump pulse energy is 5.2 nJ for (**a**) and (**c**) and 12.5 nJ for (**b**) and (**d**)

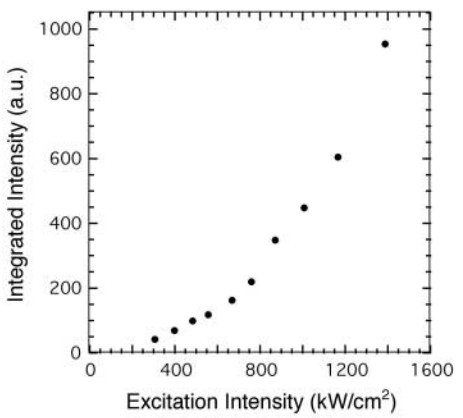

Fig. 8. Spectrally integrated intensity of emission from the ZnO powder film versus the excitation intensity

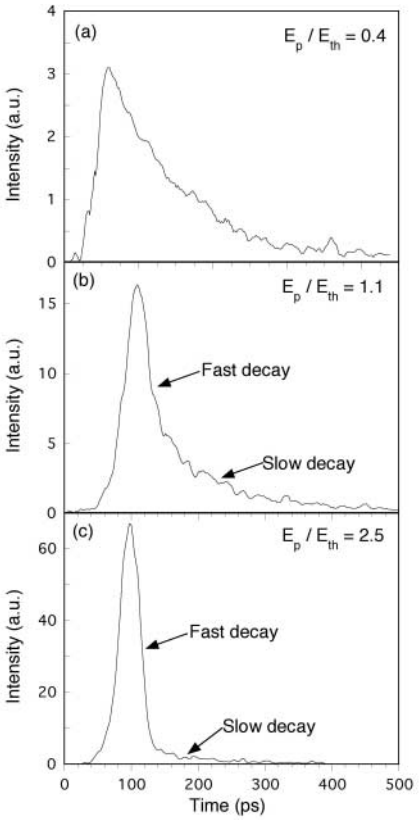

Fig. 9. Temporal evolution of emission from ZnO powder film. The incident pump pulse energy is (**a**) 2.8 nJ, (**b**) 5.5 nJ, and (**c**) 8.9 nJ

shortened significantly. By curve fitting, we find that the exponential decay of emission consists of a fast component and a slow component. As shown in Fig. 9b, the initial decay of emission is quite fast. The decay time is 27 ps. After $\sim$ 50 ps, the fast decay is replaced by slow decay. The latter decay time is 167 ps, which is equal to the emission decay time below the lasing threshold. Since the sample is pumped by 20-ps pulses, the optical gain is transient. Laser oscillation occurs in a short time after each pump pulse. The strong laser emission depletes the population inversion quickly. When the optical gain is reduced below the loss, laser oscillation stops. Laser emission is replaced by spontaneous emission. Hence, the initial fast decay corresponds to laser emission, and the later slow decay is due to spontaneous emission. As the pump power is increased further, the initial laser emission becomes much stronger than the later spontaneous emission, as shown in Fig. 9c. When the pump power exceeds the threshold, the emission pulse is dramatically shortened from 200 to 30 ps. From the threshold behavior of the emission intensity,

the emergence of very narrow spectral peaks, and the dramatic shortening of the emission pulses, we conclude that lasing has occurred in the ZnO powder film. Similar lasing phenomena have been observed in ZnO polycrystalline films and GaN powder.

The experimental fact that the bright spots in the emission pattern and the lasing modes in the emission spectrum always appear simultaneously suggests that the bright spots are related to the laser light. There are two possible explanations for the bright spots. One is that the laser light intensity at the locations of the bright spots is high. The other is that the laser light is not particularly strong at the locations of the bright spots. However, there are some efficient scattering centers at the locations of the bright spots, and thus, the laser light is strongly scattered. In the latter case, these scattering centers should also strongly scatter the spontaneously emitted light below the lasing threshold because scattering is a linear process. Hence, these bright spots should exist below the lasing threshold. However, there are no bright spots below the lasing threshold. Therefore, these bright spots are not caused by efficient scatterers, but by strong laser light in the medium.

Next we present an explanation for our experimental data. The short transport mean free path indicates very strong light scattering in the powder film. However, the transport mean free path obtained from the coherent backscattering measurement is an average over a large volume of the sample. Due to the local variation of particle density and spatial distribution, there exist small regions of higher disorder and stronger scattering. Light can be confined in these regions through multiple scattering and interference. For a particular configuration of scatterers, only light at certain wavelengths can be confined because the interference effect is wavelength sensitive. In a different region of the sample, the configuration of the scatterers is different, and thus, light at different wavelengths is confined. In other words, some quasi-states are spatially localized in small regions, and they have relatively long lifetimes. When the optical gain reaches the loss of such a quasi-state, lasing action occurs in the quasi-state. The lasing peaks in the emission spectrum illustrate the frequencies of the quasi-states, and the bright spots in the spatial light pattern exhibit the positions and shapes of the quasi-states.

Unlike conventional lasers with directional output, laser emission from random media can be observed in all directions. However, the laser emission spectra vary with the observation angle. Since different quasi-states have different output directions, lasing modes observed at different angles are different.

Although the data presented above indicate that lasing has occurred in the ZnO powder, the final proof of a laser comes from coherence and statistics measurement. Next, I will present our photon statistics measurement result which shows that indeed coherent light is generated from the disordered medium.

ZnO nanoparticles are cold pressed under a pressure of 200 MPa to form a pellet 2 mm thick. From the coherent backscattering experiment, we estimate that $l \sim 2.3\lambda$. Under the optical pumping of a mode-locked Nd:YAG laser, the emission from the ZnO pellet is collected by a lens and focused to the entrance slit of a 0.5-m Jarrell–Ash spectrometer. The output port of the spectrometer is connected to a Hamamatsu streak camera whose entrance slit is perpendicular to that of the spectrometer. The photocathode width of the streak camera gives an observable spectral window of 6.7 nm with a spectral resolution of 0.1 nm. Partial output of the pump laser goes directly to a fast photodiode whose output signal triggers the streak camera. A Peltier-cooled CCD camera, operating at $-50°$ C for reduced dark noise, is used to record the streak image. The streak camera operates in the photon counting mode. A threshold is set to eliminate the contribution of the dark-current noise. Thus, in the absence of an input signal, no photons are counted.

By combining the spectrometer with the streak camera, we are able to separate different lasing modes and measure the temporal evolution of each mode. Figure 10 is a 2-D image taken by the CCD camera. The horizontal axis is the time, and the vertical axis is the wavelength. When the pump power exceeds a threshold, discrete lasing modes appear in the spectrum. For different modes, lasing starts at different times and lasts for different periods of time. Such dynamic behavior is caused by different decay rates of the quasi-states that have lased.

Next, we measure the photon statistics of a single lasing mode. In the 2-D image shown in Fig. 10, we draw a rectangle, one of whose sides is wavelength interval $\delta\lambda$ and the other side is time interval δt. The number of photons inside this rectangle is counted for each pulse. After collecting photon count data for a large number of pulses, the probability $P(n)$ of n

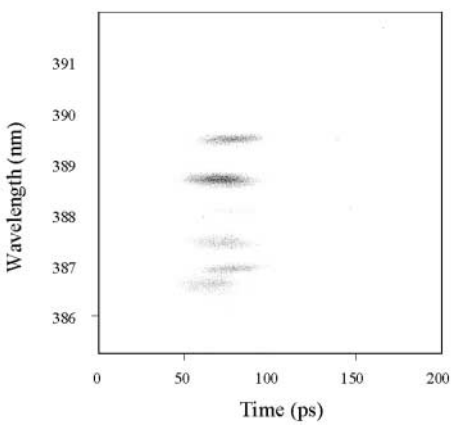

Fig. 10. The measured spectral-temporal image of the emission from a ZnO pellet. The incident pump pulse energy is 4.5 nJ

photons within $(\lambda, \lambda + \delta\lambda)$ and $(t, t + \delta t)$ is obtained. The frequency interval $\delta\nu$ of the counting area is calculated from λ and $\delta\lambda$. When $\delta\nu \cdot \delta t \leq 1$, the counting area corresponds to a single electromagnetic (EM) mode. For coherent light, the photon number distribution $P(n)$ in a single mode satisfies Poisson distribution $P(n) = \langle n\rangle^n \mathrm{e}^{-\langle n\rangle}/n!$, where $\langle n\rangle$ is the average photon number. For chaotic light, the photon number distribution $P(n)$ in a single mode satisfies the Bose–Einstein distribution $P(n) = \langle n\rangle^n/(1 + \langle n\rangle)^{n+1}$. Note that the above distribution holds only for a single mode. In multimode chaotic light, the photon number distribution approaches Poisson distribution. From $P(n)$, we obtain the normalized second-order correlation coefficient $G_2 = 1 + \left[\langle(\Delta n)^2\rangle - \langle n\rangle\right]/\langle n\rangle^2$. For the Poisson distribution, $G_2 = 1$. For the Bose–Einstein distribution, $G_2 = 2$.

We measured the photon statistics of coherent light and chaotic light to confirm the reliability of the spectrometer–streak camera setup for the photon statistics measurement. Then, we moved to the photon statistics measurement of random lasers with coherent feedback. The pump intensity is above the threshold where discrete spectral peaks appear, so that we can measure the photon statistics of a single peak. In the 2-D spectral-temporal image of ZnO emission, we pick up one of the brightest peaks and count the number of photons within the area of $(\lambda_0 - \Delta\lambda/2, \lambda_0 + \Delta\lambda/2)$ and $(t_0 - \Delta t/2, t_0 + \Delta t/2)$ for each pulse. λ_0 is the center wavelength of the spectral peak we choose, and t_0 is the time when the intensity of the emission pulse at λ_0 is maximum. $\Delta\lambda = 0.12\,\mathrm{nm}$, and $\Delta t = 3.9\,\mathrm{ps}$. The corresponding $\Delta\nu = 2.4 \times 10^{11}\,\mathrm{Hz}$, and hence, $\Delta\nu \cdot \Delta t = 0.95$. There are 100 CCD pixels within the area of $(\lambda_0 - \Delta\lambda/2, \lambda_0 + \Delta\lambda/2)$ and $(t_0 - \Delta t/2, t_0 + \Delta t/2)$. If two photons from the same pulse hit the same pixel, the count is one instead of two. Hence, such events cause error in the photon counting. To eliminate this kind of error, the photons that hit the pixels must be sparse enough that the probability of two photons hitting the same pixel is negligible. When the ZnO emission is strong, we use neutral density filters to attenuate the signal, so that the percentage of the pixels that are hit by the photons during each pulse is below 5 %.

Figure 11a shows the measured photon statistics at the threshold where discrete spectral peaks appear. From the data of $P(n)$, we calculate the count mean $\langle n\rangle$ and obtain the Bose–Einstein distribution. The measured photon number distribution is very close to the Bose–Einstein distribution for the same mean photon number. Using the data of $P(n)$, we also calculate $G_2 = 1.94$. As we increase the pump intensity, the photon statistics of ZnO emission starts deviating from the Bose–Einstein statistics. As shown in Fig. 11b, when the pump intensity is 1.5 times the threshold, the measured photon number distribution is between the Bose–Einstein distribution and the Poisson distribution for the same mean photon number. G_2 becomes 1.51. When the pump intensity is increased to three times the threshold, the photon number distribution of ZnO emission gets closer to the Poisson distri-

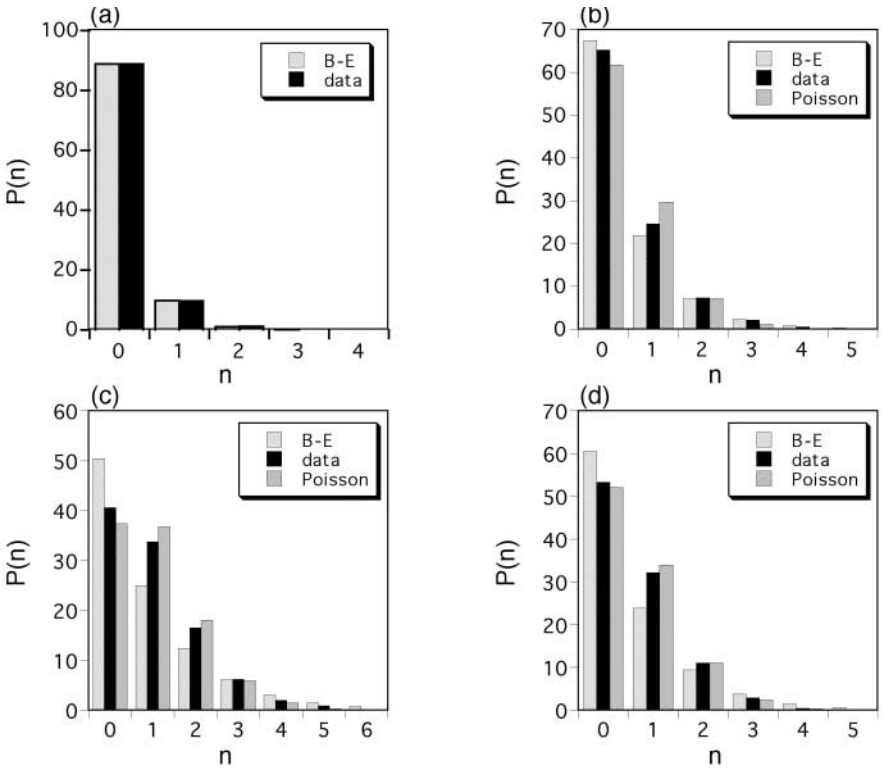

Fig. 11. The solid columns are the measured photon count distributions of the emission from the ZnO pellet. The *dotted* (*dashed*) columns are the Bose–Einstein (Poisson) distributions for the same count mean. The incident pump intensity is (**a**) 1.0, (**b**) 1.5, (**c**) 3.0, (**d**) 5.6 times the threshold intensity where discrete spectral peaks appear

bution (Fig. 11c). G_2 is reduced to 1.19. Eventually, when the pump intensity is 5.6 times the threshold, the photon number distribution is nearly identical to the Poisson distribution (Fig. 11d). The corresponding G_2 is 1.06.

Figure 12 shows the value of second-order correlation coefficient G_2 as a function of pump intensity. As the pump intensity increases, G_2 decreases gradually from 2 to 1. The error bar in Fig. 12 results from the finite number of samplings in the measurement. Figures 11 and 12 illustrate that the photon statistics of emitted light from a ZnO pellet changes continuously from Bose–Einstein statistics at the threshold to Poisson statistics well above the threshold. Therefore, the light field in the random medium has undergone a second-order phase transition.

The photon statistics of a random laser with resonant feedback is very different from that of a random laser with nonresonant feedback. The random laser with nonresonant feedback consists of many low-Q modes that are

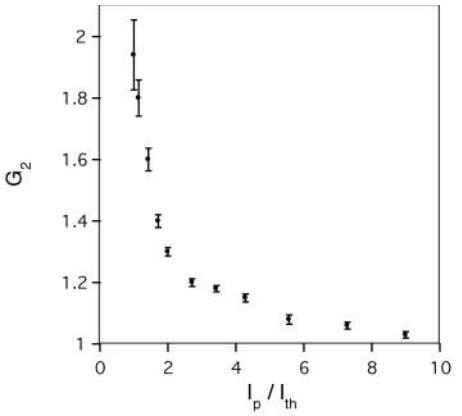

Fig. 12. The second-order correlation coefficient G_2 as a function of the ratio between the incident pump intensity I_p and the threshold intensity I_th

strongly coupled. The fluctuation of the total number of photons in all modes of laser emission is smaller than that of blackbody radiation with the same number of modes [26]. The stabilization of the total photon number results from the gain saturation effect. However, the photon number distribution in each mode remains Bose–Einstein distribution even well above the threshold. Strong mode coupling prevents stabilization of the photon number in individual modes. In contrast, for a random laser with resonant feedback, the number of photons in each lasing mode is stabilized well above the threshold by the gain saturation effect. This phenomenon indicates very weak coupling among lasing modes. The difference in the photon statistics of the two kinds of random lasers originates from different scattering strength in the random medium. When optical scattering is weak, the modes are strongly coupled. As the amount of scattering increases, the interaction of the modes decreases. In fact, the decoupling of the modes is an indication of incipient photon localization. Although a random laser with resonant feedback is a multimode laser, it behaves like an ensemble of almost independent single-mode lasers.

4 Microlasers Made of Disordered Media

Disorder-induced optical scattering provides coherent feedback for lasing and also leads to spatial confinement of light in micrometer-sized volume. Utilizing this new physical mechanism of optical confinement, we fabricated microlasers with a disordered medium [27].

The micrometer-sized random material is made of ZnO nanocrystallites. Specifically, 0.05 mol of zinc acetate dihydrate is added to 300 ml diethylene glycol. The solution is heated to 160° C. As the solution is heated, more zinc acetate is dissociated. When the Zn^{2+} concentration in the solution exceeds

the nucleation threshold, ZnO nanocrystallites precipitate and agglomerate to form clusters. The size of the clusters can be controlled by varying the rate at which the solution is heated. The average size of ZnO nanocrystallites ~ 50 nm. The size of the clusters varies from submicron to a few microns [28].

The inset of Fig. 13 is the SEM image of a typical ZnO cluster. The size of the cluster is about 1.7 μm, and it contains roughly 20000 ZnO nanocrystallites. The ZnO cluster is optically pumped by the fourth harmonic of a mode-locked Nd:YAG laser. The pump light is focused by a microscope objective onto a single cluster. The spectrum of emission from the cluster is measured by a spectrometer with 0.13 nm spectral resolution. Simultaneously, the spatial distribution of the emitted light intensity in the cluster is imaged by a ultraviolet (UV) microscope onto a UV-sensitive CCD camera. A band-pass filter is placed in front of the microscope objective to block the pump light.

We performed optical measurement of the cluster shown in Fig. 13. At low pump power, the emission spectrum consists of a single broad spontaneous emission speak (Fig. 14a). Its FWHM is 12 nm. The spatial distribution of the spontaneous emission intensity is uniform across the cluster (Fig. 14b). When the pump power exceeds a threshold, a sharp peak emerges in the emission spectrum shown in Fig. 14c. Its FWHM is 0.22 nm. Simultaneously, a couple of bright spots appear in the image of the emitted light distribution in the cluster in Fig. 14d. The size of the bright spot is ~ 0.3 μm. When the pump power is increased further, a second sharp peak emerges in the emission spectrum (see Fig. 14e). Correspondingly, additional bright spots appear in the image of the emitted light distribution in Fig. 14f.

As shown in Fig. 13, above the pump intensity at which sharp spectral peaks and bright spots appear, the emission intensity increases much more

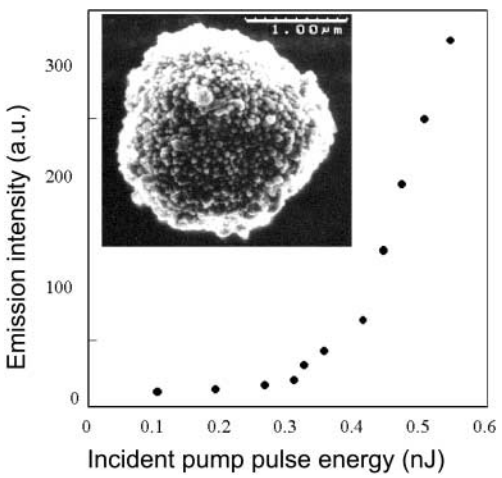

Fig. 13. Spectrally integrated intensity of emission from a ZnO cluster versus the incident pump pulse energy. The inset is the SEM image of a ZnO cluster

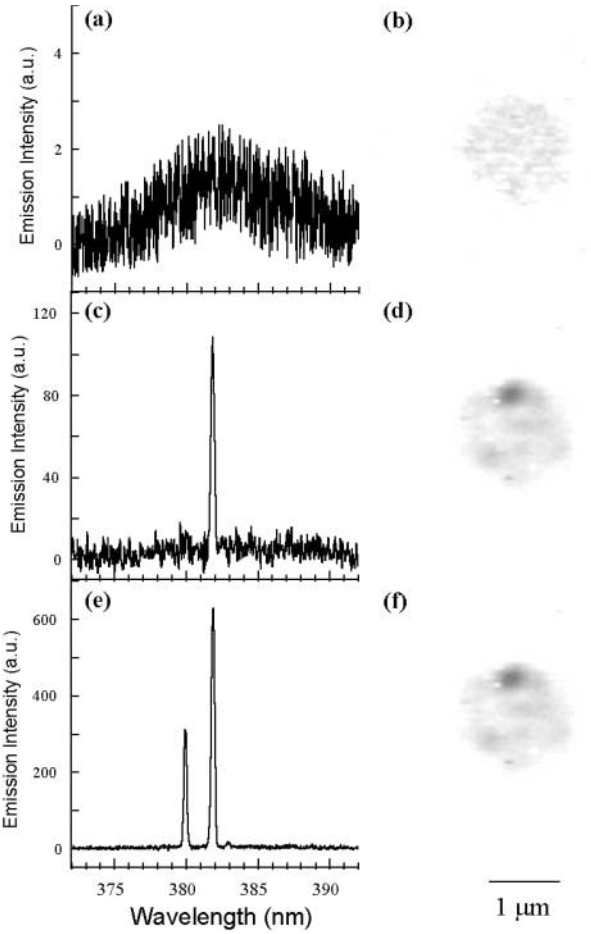

Fig. 14. (**a**), (**c**), and (**e**) The spectra of emission from the ZnO cluster shown in Fig. 1. (**b**), (**d**), and (**f**) The corresponding spatial distributions of emission intensity in the cluster. The incident pump pulse energy is 0.26 nJ for (**a**) and (**b**), 0.35 nJ for (**c**) and (**d**), and 0.50 nJ for (**e**) and (**f**)

rapidly with the pump intensity. These data suggest that lasing action has occurred in the micrometer-sized cluster. The incident pump pulse energy at the lasing threshold is ~ 0.3 nJ. Note that only $\sim 1\%$ of the incident pump light is absorbed. The rest is scattered.

Since the cluster is very small, optical reflection from the boundary of the cluster might have some contribution to light confinement in the cluster. However, the laser cavity is not formed by total internal reflection at the boundary. Otherwise, the spatial pattern of laser light would be a bright ring near the edge of the cluster [29]. We believe that 3-D confinement of laser light in the micrometer-sized ZnO cluster is achieved through disorder-

induced scattering and interference. Since the interference effect is wavelength sensitive, only light at certain wavelengths can be confined in the cluster. To check that the main mechanism of optical confinement is not light reflection at the surface of the cluster, we chose some clusters with irregular shape and rough surface and repeated the above measurement.

Figure 15 presents the measurement result of a second cluster with irregular shape. It is slightly larger than 1 μm. Similar lasing phenomenon is observed in this cluster. The incident pump pulse energy at the lasing threshold is ~ 0.2 nJ. The FWHM of the emission spectrum narrows dramatically from 12 nm below the lasing threshold to 0.16 nm above the lasing threshold (Fig. 15b). After taking into account the instrumental broadening, the actual line width of the lasing mode is only 0.09 nm. Bright spots appear in the image of laser light distribution in the cluster. By adjusting the microscope objective, light distribution on a different plane inside the cluster is imaged onto the CCD camera. Figure 15c,d are the images of light distribution on two planes with different depths inside the cluster. Some bright spots appear in one image, but not in the other. This suggests that these bright spots are buried at different depths inside the cluster. Because lasing can occur in ZnO clusters with irregular shape and rough surfaces, we confirm that the optical

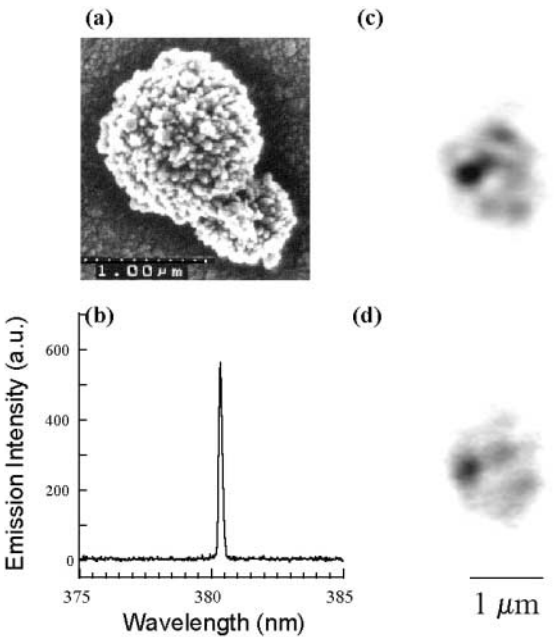

Fig. 15. (**a**) The SEM image of a second ZnO cluster. (**b**) The spectrum of emission from this cluster above the lasing threshold. The incident pump pulse energy is 0.27 nJ. (**c**) and (**d**) The spatial distribution of emission intensity in the cluster at the same pump power

confinement is not caused by reflection at the surface of the cluster, but by scattering inside the cluster.

Finally, I would like to compare the powder microlaser with other types of microlasers. Microlasers have important applications to integrated photonic circuits. Over the past decade, several types of microlasers have been developed. The key issue for a microlaser is to confine light in a small volume with dimensions on the order of an optical wavelength. In the vertical cavity surface emitting laser, light is confined by two distributed Bragg reflectors [30]. The microdisk laser utilizes total internal reflection at the edge of a high index disk to form whispering gallery modes [31]. In the recent demonstration of a two-dimensional photonic band-gap defect mode laser, lateral confinement of light is achieved by Bragg scattering in a two-dimensional periodic structure [32]. The fabrication of these microlasers requires expensive state-of-the-art semiconductor growth and microfabrication facilities. We demonstrate a new type of microlaser which is made of a disordered medium [27]. The optical confinement is achieved through disorder-induced scattering and interference. The fabrication of such a microlaser is much easier and cheaper than that of most microlasers.

5 Theoretical Modeling

In the last section, I will briefly describe our theoretical simulation of random lasers with coherent feedback. Several models have been set up in the theoretical study of the stimulated emission in an active random medium, e. g., the diffusion equation with gain [33,34], the Monte Carlo simulation [35], and the ring laser with nonresonant feedback [36]. However, these models cannot predict lasing with coherent feedback because the phase of the optical field is neglected. We take a different approach: we directly calculate the electromagnetic field distribution in a random medium by solving the Maxwell equations using the finite-difference time-domain (FDTD) method [37]. The advantage of this approach is that we can model the real structure of a disordered medium and calculate both the emission pattern and the emission spectrum [25,38].

In our model, ZnO particles are randomly positioned in space. The particle size is 50 nm. The random medium has a finite size, and it is surrounded by air. To model the random medium located in infinitely large space, we use the uniaxial perfect matched layer (UPML) absorbing boundary condition to absorb all of the outgoing light waves in the air [39]. Using the FDTD method, we solve the Maxwell curl equations

$$\begin{aligned} \frac{\partial \boldsymbol{H}}{\partial t} &= -\frac{1}{\mu_0}\nabla \times \boldsymbol{E}\,, \\ \frac{\partial \boldsymbol{E}}{\partial t} &= \frac{1}{\epsilon}\nabla \times \boldsymbol{H} - \frac{\sigma}{\epsilon}\,\boldsymbol{E}\,, \end{aligned} \tag{1}$$

in the time domain. The randomness is introduced into the Maxwell equations through the dielectric constant ε, which varies spatially due to the random distribution of ZnO particles. We introduce optical gain by negative conductance [40]. The spectral gain profile of the dye solution is

$$\sigma(\omega) = -\frac{\sigma_0}{2}\left[\frac{1}{1+\mathrm{i}(\omega-\omega_0)T_2} + \frac{1}{1+\mathrm{i}(\omega+\omega_0)T_2}\right]. \tag{2}$$

σ_0 is related to the peak value of the gain set by the pumping level, and T_2 is the dipole relaxation time, which is inversely proportional to the spectral gain width.

In our simulation, a seed pulse, whose spectrum covers the ZnO emission spectrum, is launched in the center of the random medium at $t = 0$. When the optical gain is above the lasing threshold, the EM field oscillation builds up in the time domain. Using the discrete Fourier transform of the time domain data, we obtain the emission spectrum. Figure 16 shows the calculated emission spectrum and emission pattern for a specific configuration of scatterers. The size of the random medium is 3.2 μm. The filling factor of ZnO particles is 0.5. When the optical gain is just above the lasing threshold, the emission spectrum, shown in Fig. 16a, consists of a single peak. Figure 16b represents the light intensity distribution in the random medium. There are a few bright spots near the center. At the edge of the random medium, the light intensity is almost zero. To check the effect of the boundary, we change the spatial distribution of the scatterers near the edges of the random medium. We find that both the emission spectrum and the emission pattern remain the same. Their independence of the boundary condition indicates that the lasing mode is formed by multiple scattering and interference inside the disordered medium. When the optical gain is increased further, an additional lasing mode appears.

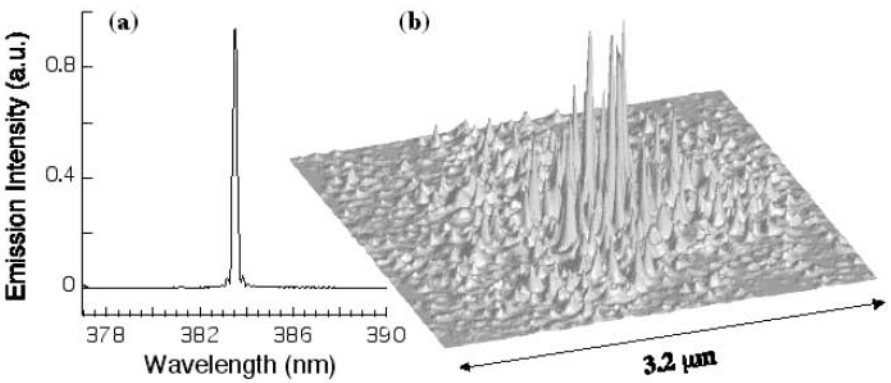

Fig. 16. (**a**) The calculated emission spectrum. (**b**) The calculated spatial distribution of emission intensity in the random medium

Our numerical simulation of random lasers with coherent feedback also confirms the second-order phase transition of the light field at the threshold. Below the lasing threshold, the seed pulse dies away from the random medium into the absorbing boundary layers. Only when the optical gain exceeds the threshold, the EM field builds up inside the random medium. Since the classical EM field represents the coherent part of a quantum field, our simulation result indicates that the quantum field in a random medium has no coherent part below the threshold; its coherent component appears only above the threshold.

6 Conclusion

In summary, we have observed lasing with resonant feedback in active random media. Recurrent light scattering provides coherent feedback for lasing. When the pump power exceeds the threshold, discrete lasing modes appear in the spectrum, the emission intensity increases suddenly, and the emission pulses are shortened dramatically. The photon statistics changes gradually from Bose–Einstein statistics at the threshold to Poisson statistics well above the threshold. Laser emission from random media can be observed in all directions.

In addition, we achieved spatial confinement of laser light in micrometer-sized random media. Since the transport mean free path is less than the optical wavelength, the optical confinement is attributed to the disorder-induced scattering and interference. Using the finite-difference time-domain method, we simulate lasing with coherent feedback in active random media. We find that the lasing modes are insensitive to the boundary conditions.

Finally, we illustrated very different lasing mechanisms for random lasers with resonant feedback and random lasers with nonresonant feedback. By varying the amount of scattering, we demonstrate the transition between the two kinds of random lasers.

Acknowledgments

I acknowledge the collaboration with R. P. H. Chang, S. T. Ho, P. Kumar, J. Y. Xu, Y. Ling, S.-H. Chang, A. Burin, H. C. Ong, E. W. Seelig, X. Liu, Y. G. Zhao, D. Z. Zhang, and J. Y. Dai. This work is supported partially by the United States National Science Foundation under Grant No. ECS-9877113, the David and Lucile Packard Foundation, and the Alfred P. Sloan Foundation.

References

1. S. John, Localization of light (in dielectric microstructures), Phys. Today **44**, 32 (1991) 303
2. M. P. van Albada, A. Lagendijk, Observation of weak localization of light in a random medium, Phys. Rev. Lett. **55**, 2692 (1985) 303, 310, 312
3. P. E. Wolf, G. Maret, Weak localization and coherent backscattering of photons in disordered media, Phys. Rev. Lett. **55**, 2696 (1985) 303, 310, 312
4. A. Z. Genack, N. Garcia, Observation of photon localization in a three-dimensional disordered system, Phys. Rev. Lett. **66**, 2064 (1991) 303
5. R. Dalichaouch, J. P. Armstrong, S. Schultz, P. M. Platzman, S. L. McCall, Microwave localization by two-dimensional random scattering, Nature **354**, 53 (1991) 303
6. D. S. Wiersma, P. Bartolini, A. Lagendijk, R. Righini, Localization of light in a disordered medium, Nature **390**, 671 (1997) 303
7. F. J. P. Schuurmans, D. Vanmaekelbergh, J. van de Lagemaat, A. Lagendijk, Strongly photonic macroporous gallium phosphide networks, Science **284**, 141 (1999) 303
8. F. J. P. Schuurmans, M. Megens, D. Vanmaekelbergh, A. Lagendijk, Light scattering near the localization transition in macroporous GaP networks, Phys. Rev. Lett. **83**, 2183 (1999) 303
9. A. A. Chabanov, M. Stoytchev, A. Z. Genack, Statistical signatures of photon localization, Nature **404**, 850 (2000) 303
10. P. W Anderson, Absence of diffusion in certain random lattices, Phys. Rev. **109**, 1492 (1958) 303
11. N. M. Lawandy, R. M. Balachandran, A. S. L. Gomes, E. Sauvain, Laser action in strongly scattering media, Nature **368**, 436 (1994) 304
12. W. Sha, C.-H. Liu, R. Alfano, Spectral and temporal measurements of laser action of Rhodamine 640 dye in strongly scattering media, Opt. Lett. **19**, 1922 (1994) 304
13. C. Gouedard, D. Husson, C. Sauteret, F. Auzel, A. Migus, Generation of spatially incoherent short pulses in laser-pumped neodymium stoichiometric crystals and powders, J. Opt. Soc. Am. B **10**, 2358 (1993) 304
14. G. van Soest, M. Tomita, A. Lagendijk, Amplifying volume in scattering media, Opt. Lett. **24**, 306 (1999) 304
15. V. S. Letokhov, Generation of light by a scattering medium with negative resonance absorption, Sov. Phys. JETP **26**, 835 (1968) 304
16. H. Cao, Y. G. Zhao, H. C. Ong, S. T. Ho, J. Y. Dai, J. Y. Wu, R. P. H. Chang, Ultraviolet lasing in resonators formed by scattering in semiconductor polycrystalline films, Appl. Phys. Lett. **73**, 3656 (1998) 304, 312
17. H. Cao, Y. G. Zhao, S. T. Ho, E. W. Seelig, Q. H. Wang, R. P. H. Chang, Random laser action in semiconductor powder, Phys. Rev. Lett. **82**, 2278 (1999) 304, 312
18. S. V. Frolov, Z. V. Vardeny, K. Yoshino, A. Zakhidov, R. H. Baughman, Stimulated emission in high-gain organic media, Phys. Rev. B **59**, 5284 (1999) 304
19. H. Cao, J. Y. Xu, S.-H. Chang, S. T. Ho, Transition from amplified spontaneous emission to laser action in strongly scattering media, Phys. Rev. B **61**, 1985 (2000) 304, 308

20. R. V. Ambartsumyan, N. G. Basov, P. G. Kryukov, V. S. Letokhov, Nonresonant feedback in lasers, in *Progress in Quantum Electronics*, J. H. Sanders, K. W. H. Stevens (Eds.) (Pergamon Press, London 1970) Vol. 1, Pt. 3, pp. 105–193 310
21. D. S. Wiersma, A. Lagendijk, Laser action in very white paint, Phys. World January, 33 (1997) 310
22. J. X. Zhu, D. J. Pine, D. A. Weitz, Internal reflection of diffusive light in random media, Phys. Rev. A **44**, 3948 (1991) 310, 313
23. H. C. Ong, R. P. H. Chang, Effect of laser intensity on the properties of carbon plasmas and deposited films, Phys. Rev. B **55**, 13213 (1997) 311
24. H. Cao, Y. G. Zhao, H. C. Ong, R. P. H. Chang, Far-field characteristics of random lasers, Phys. Rev. B **59**, 15107 (1999) 312
25. H. Cao, J. Y. Xu, D. Z. Zhang, S.-H. Chang, S. T. Ho, E. W. Seelig, X. Liu, R. P. H. Chang, Spatial confinement of laser light in active random media, Phys. Rev. Lett. **84**, 5584 (2000) 312, 324
26. R. V. Ambartsumyan, P. G. Kryukov, V. S. Letokhov, and Yu. A. Matveets, Statistical emission properties of a nonresonant feedback laser, Sov. Phys. JETP **26**, 1109 (1968) 320
27. H. Cao, J. Y. Xu, E. W. Seelig, R. P. H. Chang, Microlasers made of disordered media, Appl. Phys. Lett. **76**, 2997 (2000) 320, 324
28. D. Jezequel, J. Guenot, N. Jouini, F. Fievet, Submicrometer zinc oxide particles: Elaboration in polyol medium and morphological characteristics, J. Mater. Res. **10**, 77 (1995) 321
29. H. Taniguchi, S. Tanosaki, K. Tsujita, H. Inaba, Experimental Studies on Output, Spatial, and Spectral Characteristics of a Microdroplet Dye Laser Containing Intralipid as a Highly Scattering Medium, IEEE J. Quant. Electron. **32**, 1864 (1996) 322
30. J. L. Jewell, J. P. Harbison, A. Scherer, Y. H. Lee, L. T. Florez, Vertical-cavity surface-emitting lasers: Design, growth, fabrication, characterization, IEEE J. Quant. Electron. **27**, 1332 (1991) 324
31. S. L. McCall, A. F. J. Levi, R. E. Slusher, S. J. Pearton, R. A. Logan, Whispering-gallery mode microdisk lasers, Appl. Phys. Lett. **60**, 289 (1992) 324
32. O. Painter, R. K. Lee, A. Scherer, A. Yariv, J. D. O'Brien, P. D. Dapkus, I. Kim, Two-dimensional photonic band-gap defect mode laser, Science **284**, 1819 (1999) 324
33. D. S. Wiersma, A. Lagendijk, Light diffusion with gain and random lasers, Phys. Rev. E **54**, 4256 (1996) 324
34. S. John, G. Pang, Theory of lasing in a multiple-scattering medium, Phys. Rev. A **54**, 3642 (1996) 324
35. G. A. Berger, M. Kempe, A. Z. Genack, Dynamics of stimulated emission from random media, Phys. Rev. E **56**, 6118 (1997) 324
36. R. M. Balachandran, N. M. Lawandy, Theory of laser action in scattering gain media, Opt. Lett. **22**, 319 (1997) 324
37. A. Taflove, *Computational Electrodynamics: The Finite-Difference Time Domain Method* (Artech House, Boston 1995) 324
38. X. Y. Jiang, C. M. Soukoulis, Time dependent theory for random lasers, Phys. Rev. Lett. **85**, 70 (2000) 324

39. Z. S. Sacks, D. M. Kingsland, R. Lee, J. F. Lee, A perfectly matched anisotropic absorber for use as an absorbing boundary condition, IEEE Trans. Antenna Propagation **43**, 1460 (1995) 324
40. S. C. Hagness, R. M. Joseph, A. Taflove, Subpicosecond electrodynamics of distributed Bragg reflector microlasers: Results from finite difference time domain simulations, Radio Sci. **31**, 931 (1996)

325

Index